Combined Buoyancy-Thermocapillary Convection

Final Report

NASA Grant NAG8-715 01

G. M. Homsy
Department of Chemical Engineering
Stanford University
Stanford, CA 94305

Summary

This is a summary of work done under our NASA grant to study combined buoyancy-thermocapillary convection in two and three dimensions. Two postdoctoral fellows, Pascale Gillon and N. Ramanan, were supported during the grant period, and worked on experimental and numerical aspects of thermocapillary convection in cavities, respectively. Dr. Gillon has a position with CNRS, France, and Dr. Ramanan is currently with Fluid Dynamics, International, Chicago.

Fluid motion caused by thermally induced tension gradients on the free surface of a fluid is termed thermocapillary convection. It is well-known that in containerless processing of materials in space, thermocapillary convection is a dominant mechanism of fluid flow. Welding and crystal growth processes are terrestrial applications where thermocapillary convection has direct relevance. In recent years, an extensive body of research has been focused on this subject.

Experiments - (Dr. Pascale Gillon)

Consider the cavity sketched in Figure 1, filled with a Boussinesq fluid, heated at constant wall temperatures from the side, with insulated top and bottom, and a single free surface at which surface tension acts. Under these circumstances the flow is governed by the following dimensionless parameters.

$A_1 = h/d$	Aspect ratio
$A_2 = l/d$	Aspect ratio
$Pr = \nu / \kappa$	Prandtl number
$Ra = g \alpha \Delta T \ h^3 / \nu \kappa$	Rayleigh number
$Ma = \gamma_T \ \Delta T \ d \ / \mu \kappa$	Marangoni number
$Ca = \gamma_T \ \Delta T / \gamma$	Capillary number
Θ	Contact angle

We conducted an experimental study of thermocapillary convection in a cavity, full details of which are contained in the manuscript "Combined Thermocapillary-Buoyancy Convection in a Cavity: An Experimental Study" by Gillon and Homsy (1989), appended to this report. We give a summary of the primary results of the study here.

In contrast to the fairly extensive studies of other cavity flows, our understanding of thermocapillary cavity flow in the absence of gravity remains primitive. Simple parallel flow solutions with conductive temperature profiles that apply for low aspect ratio and low Prandtl number may be easily obtained. Numerical analysis of strongly convective thermocapillary flows by Zebib, Homsy, & Meiburg(1985) and Carpenter & Homsy(1990) in a cavity of unit aspect ratio has established that, in the limit of large Marangoni number, a finite temperature gradient remains over the entire free surface. This in turn leads to a global flow structure that is identical to that of the so-called "driven cavity" problem, i.e. a central thermocapillary vortex of constant vorticity and constant temperature, adjacent to viscous, heat conducting boundary layers near the free and no-slip boundaries of the cavity. This structure is robust, and occurs as Ma -> ∞ , regardless of the Prandtl number, although the evolution of the structure as Ma is increased is highly Prandtl number dependent, Carpenter & Homsy(1989).

It is natural to also enquire into the structure of two-dimensional thermocapillary-buoyancy driven flow, where both surface tension gradients and buoyancy contribute to the motion. We refer to this hereafter as "combined convection". This is an interesting question, since the two distinct limits of a buoyancy dominated structure on the one hand and the thermocapillary structure on the other are so different. This issue is addressed in detail in the computational study of Carpenter & Homsy(1989), in which it is concluded that thermocapillarity dominates all such cavity problems, in the limit of fixed ratio of Rayleigh to Marangoni numbers, as either one tends to infinity. Our interest is in the experimental study of such combined flows. We conducted experiments on combined buoyancy-thermocapillary convection in a cavity under circumstances in which the two mechanisms are of comparable importance in driving the convection. As is well-known, this requires working in small dimension systems on earth. The relative importance of these two mechanisms is governed by the Rayleigh and Marangoni numbers, respectively. The Prandtl number, the cavity aspect ratio, and the ratio of Rayleigh to Marangoni numbers were all held fixed at 8.4, 0.7 x 3, and 2.5 respectively; the primary experimental variable was the imposed temperature difference, which varied from 0.3 ^{o}C to 20 ^{o}C, resulting in a range of Marangoni numbers between 6 x 10^3 and 5 x 10^5. A combination of flow visualization and quantitative velocimetry with laser methods was employed.

Our experimental results may be summarized as follows. For low Marangoni numbers, the flow is steady and two-dimensional, as expected. The global nature of the flow is in good agreement with available numerical simulations of combined thermocapillary-buoyancy driven convection, as discussed in Section B below. Figure 2 gives an example of a steady two dimensional flow, made visible by illumination of tracer particles in a plane of the flow by a laser sheet.

At higher Marangoni number, $Ma > 1.5 \times 10^5$, we observed a transition to steady three dimensional convection. Examples of streak photographs taken in a plane perpendicular to the heated and cooled walls is shown in Figure 3, showing peculiar features such as the apparent interior stagnation point. The nature of this transition was found to be typical of an imperfect bifurcation, and the flow structure was investigated, both qualitatively and quantitatively. It was concluded that, for the parameter values studied, the first unstable mode consists of steady three dimensional vortical structures that are spatially periodic along the axis of the cell. Figure 4 shows a visualization of this motion, taken by illuminating the cell in the mid-plane parallel to its long axis. This mode of instability is unexpected, as it contrasts sharply with what occurs for both pure buoyancy-driven convection, and thermocapillary convection in liquid bridges. Our observations represent the discovery and first detailed study of such transitions in cavities.

Simulations - (N. Ramanan)

In order to understand the experimental observations from a theoretical point of view, it is necessary to first study the steady, two dimensional flow, and then the observed instability. Large scale simulations are particularily useful in this regard, as the interesting dynamics typically occurs in ranges of the parameters, Rayleigh, Marangoni numbers, etc. that are outside the range of analytical description. Accordingly, we undertook some simulations of the observed flows by integration of the coupled Boussinesq equations governing the steady two dimensional velocity and temperature fields. Finite difference methods, employing as many as 256x256 grid points, and multi-grid acceleration techniques were used. We report here on two of the cases studied. The only parameter that is different between the experiment and simulation is the contact angle, which is assumed to be 90 degrees in the simulation and is approximately 50 degrees in the experiment.

Case 1. Ma = 6630. Ra = 15,900. Pr = 8.4.

In Figures 5a-c, we show experimental streaklines, computed streamlines, and thermal fields for the parameters given. As can be seen, there is general qualitative agreement in the streakline comparison. The thermal field is shown as an indication of the importance of non-linear convective phenomena in these flows; in a conductive situation, the isotherms would all be vertical. In Figure 5d, we show a quantitative comparison between the computed horizontal velocity at the mid-plane of the cavity, and that measured by laser-speckle velocimetry. As can be seen, there is generally good agreement.

Case 2. Ma = 17,000. Ra = 42,500. Pr = 8.4

Figures 6a-d give the same set of comparisons as for Case 1 above. As can be seen the streaklines and streamlines are again in qualitative agreement, and the isotherms show the effects of increasingly strong convection. The quantitative agreement in velocity is not as good as Case 1, with the simulations predicting a stronger flow than is observed. Since the experimental flow is known to be steady and two-dimensional, we ascribe these differences to differences in contact angle, as follows. A contact angle of 90 degrees, as assumed in the calculations, allows the imposed temperature difference to have its gradient lie entirely in the plane of the interface, thus maximizing the thermocapillary driving force. Contact angles of greater or less than 90 degrees will have some component of the temperature gradient perpendicular to the interface, thus lessening the thermocapillary stress. The observations are consistent with this explanation.

References

Carpenter, B. M. & G. M. Homsy (1989) "Combined Buoyant-Thermocapillary Convection in a Cavity" *J. Fluid Mech.* **207**, 121.

Carpenter, B. M. & G. M. Homsy (1990) "High Marangoni Convection in a Square Cavity. Part II" *Phys. Fluids A* **2**, 137.

Gillon, P. & G. M. Homsy (1989) "Combined Thermocapillary-Buoyancy Convection in a Cavity: An Experimental Study" Unpublished manuscript and appendix to this report.

Zebib, A., G. M. Homsy, & E. Meiburg (1985) "High Marangoni Convection in a Square Cavity" *Phys. Fluids* **28**, 3549.

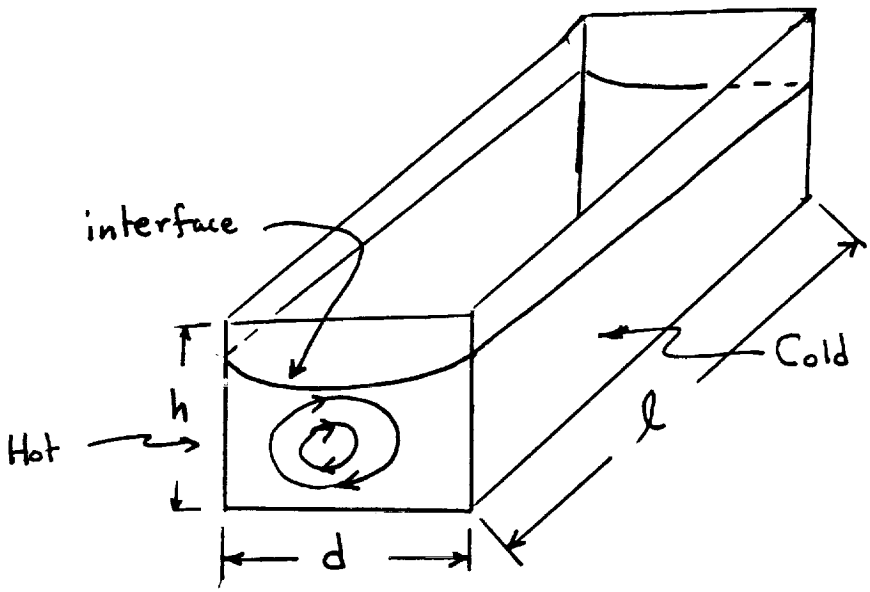

Figure 1. Schematic of experimental apparatus

Figure 2. Example of two-dimensional flow, made visible by streak photography

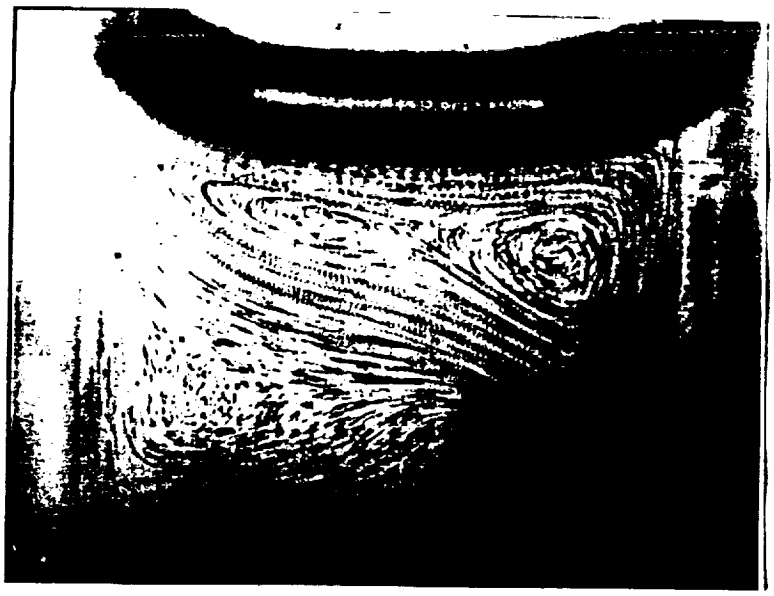

Figure 3. Streak photograph of convection pattern at high Marangoni number. Note the internal saddle point, a feature peculiar for a two dimensional flow.

Figure 4. Streak photograph along the long axis of the apparatus, showing axially-periodic steady three-dimensional flow.

(A)

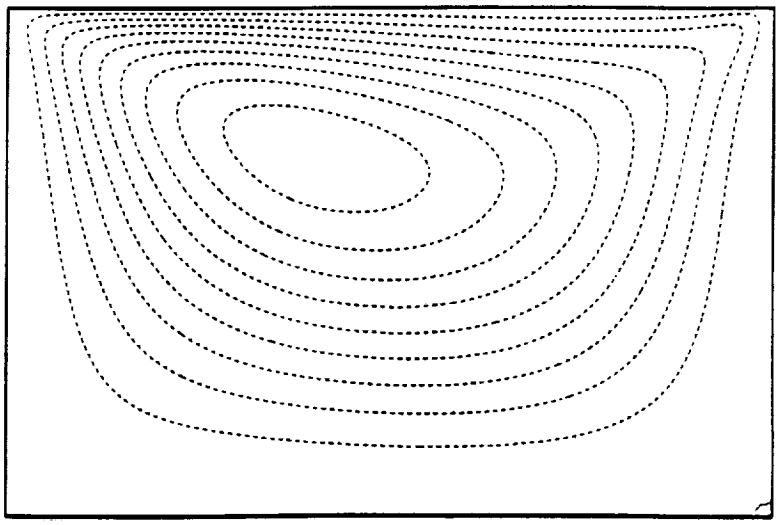

Streamfunction

Ma=6600, G=2.4, Pr=8.4, 65, bermuda

(B)

Figure 5. Comparison between simulations and experiments for Ma = 6600.
5a. Experimental streak photograph: 5b. Simulation streamlines.

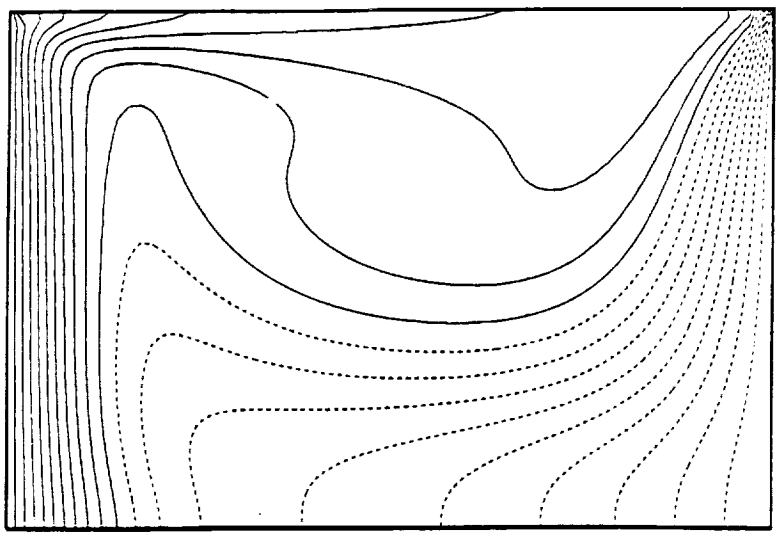

Temperature

Ma=6600, G=2.4, Pr=8.4, 65, bermuda

(C)

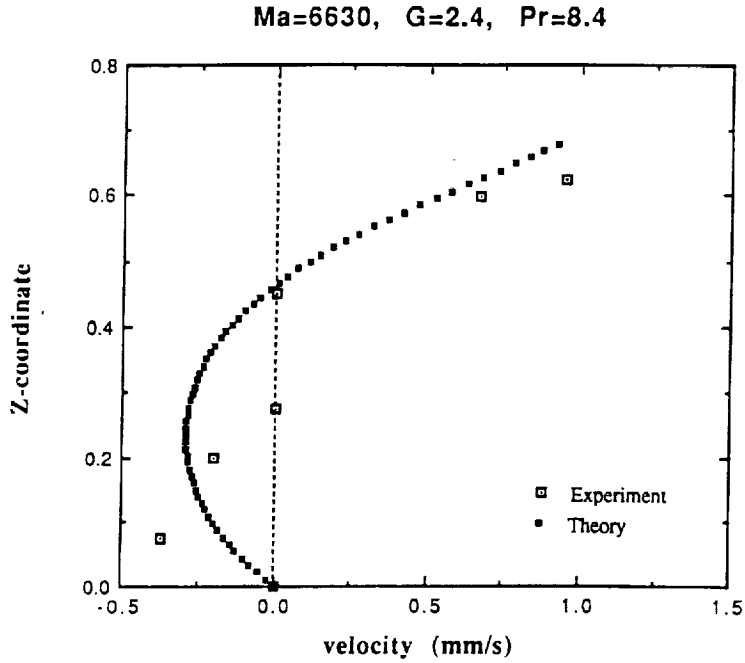

(D)

Figure 5(cont.). Comparison between simulations and experiments for Ma = 6600.
5c. Isotherms from simulation: 5d. Comparison of velocity profiles through the midplane.

(A)

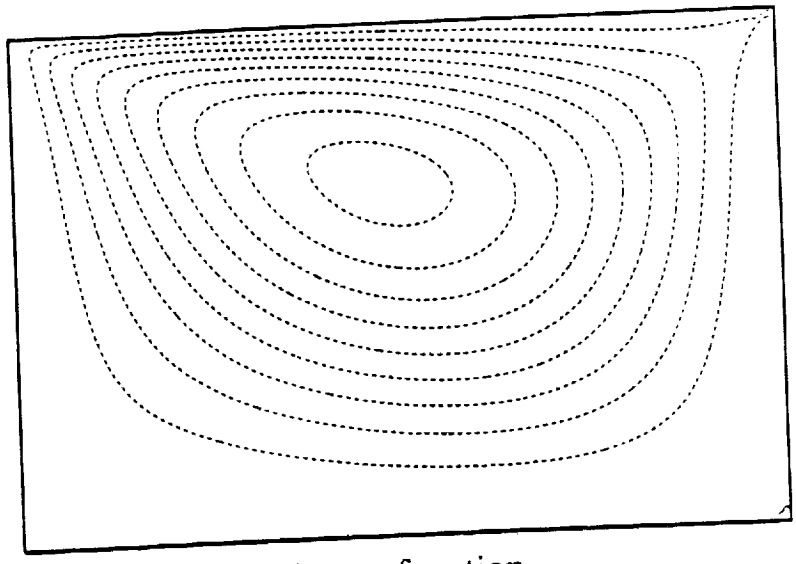

(B)

Figure 6. Comparison between simulations and experiments for Ma = 17,000.
6a. Experimental streak photograph: 6b. Simulation streamlines.

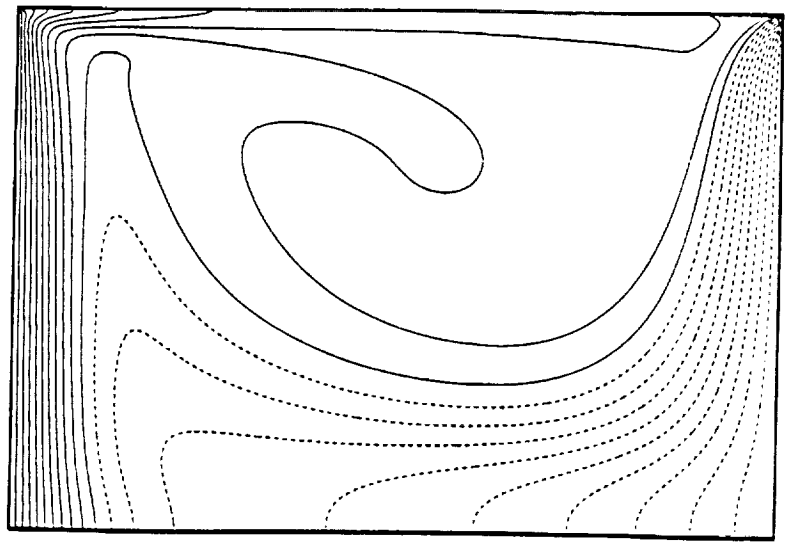

Temperature

Ma=17000, G=2.5, Pr=8.4, 129x129

(C)

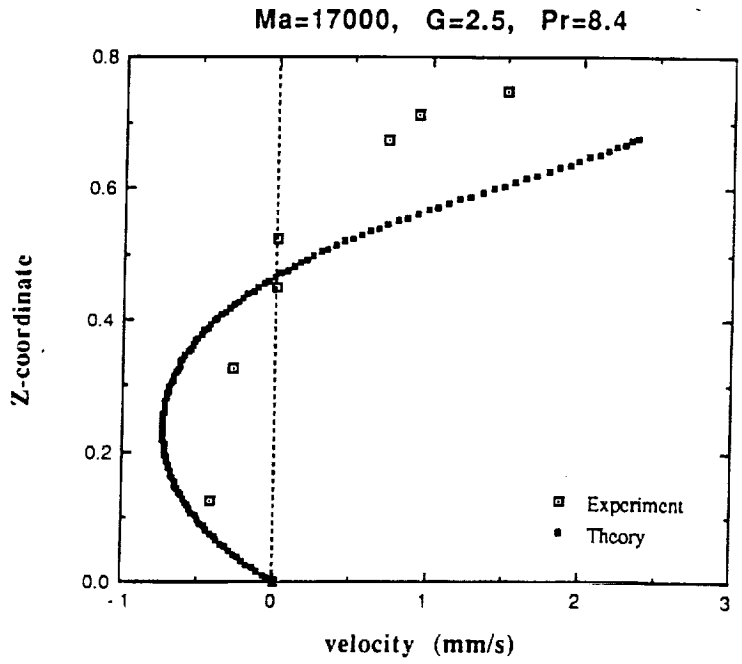

(D)

Figure 6 (cont.). Comparison between simulations and experiments for Ma = 17,000. 6c. Isotherms from simulation: 6d. Comparison of velocity profiles through the midplane.

Combined Thermocapillary-Buoyancy Convection in a Cavity:

An Experimental Study

by

Pascale Gillon & G. M. Homsy
Department of Chemical Engineering
Stanford University
Stanford CA 94305

Abstract

Convection in a cavity with a free surface and heated from the side is studied by a combination of flow visualization and particle image velocimetry. In these experiments, buoyancy and thermocapillarity are of comparable importance in driving the convection. The Prandtl number of the working fluid, the cavity aspect ratio, and the ratio of Rayleigh to Marangoni numbers are all held fixed; the primary experimentally varied parameter is the imposed temperature difference, which varied from 0.3 ^{o}C to 20 ^{o}C, resulting in a range of Marangoni numbers between 6×10^3 and 5×10^5. For low Marangoni numbers, the flow is steady and two-dimensional, as expected. The global nature of the flow is in good agreement with available numerical simulations of combined thermocapillary-buoyancy driven convection. At higher Marangoni number, $Ma > 1.5 \times 10^5$, we observe a transition to steady three dimensional convection. The nature of this transition is typical of an imperfect bifurcation, and the flow structure is investigated, both qualitatively and quantitatively. It is concluded that, for the parameter values studied, the first unstable mode consists of steady three dimensional vortical structures that are periodic along the axis of the cell. This mode of instability is unexpected, as they contrast sharply with what occurs for both pure buoyancy-driven convection, and thermocapillary convection in liquid bridges. Thus, our observations represent the discovery and first detailed study of such transitions in cavities.

1. Introduction

The study of cavity flows plays a central role in the understanding of confined fluid motions. As a result, much work has been devoted to the study of cavity flows that are driven by the motion of one of the boundaries on the one hand, (the so-called "driven cavity problem"), and by natural convection associated with lateral heating on the other. In the former case, much experimentation and numerical analysis has shown that, at high Reynolds numbers, the primary flow structure consists of a rotational inviscid flow, separated by viscous boundary layers on all walls. When the streamlines close outside of these boundary layers, the hypotheses of the Prandtl-Batchelor theorem are met, and the inviscid core is in solid body rotation; see Ghia, Ghia,& Shin(1982), Schreiber & Keller(1983), Kim & Moin(1985), among others. This global flow structure has been established by numerical analysis, and the study of the stability and transition of the two dimensional flow is a subject of current interest, see for example, Kim & Moin(1985), Koseff & Street(1984 a,b).

On the other hand, natural convective cavity flows driven by lateral heating are characterized by buoyancy layers into which the streamlines penetrate, and the inviscid non heat-conducting core is characterized by open streamlines, non constant vorticity, and a vertically stratification, as first discussed by Gill(1966) and elaborated upon by Walker & Homsy(1978)in the slightly different context of convection in porous media. The study of transition and instability in such cavity problems began with the seminal work of Hart(1971,1972), and is now fairly advanced from both an experimental and computational point of view; see, for example, Drummond & Korpela(1987), Simpkins & Dudderar(1981), and references therein. Depending upon parameters such as Prandtl number and aspect ratio, the basic convective vortex can become unstable to either steady or time-dependent two-dimensional motions, as well as steady three-dimensional longitudinal rolls. The critical points for these transitions are known for some regions of parameter space, but a complete characterization remains to be done. Nonlinear convective states past these critical points are generally characterized by a structure closely related to the neutral modes at transition, suggesting, but not proving, that these are all supercritical bifurcations.

Our interest is in the study of cavity flows when surface tension gradients contribute to driving the flow. Consider the cavity sketched in Figure 1, filled with a Boussinesq fluid, heated at constant wall temperatures from the side, with insulated top and bottom, and a single free surface at which surface tension acts. It is characterized by the usual parameters of coefficient of thermal expansion, viscosity, heat conductivity and heat capacity, coefficient of variation of surface tension with temperature, etc. Under these circumstances, scaling of the equations or use of dimensional

analysis indicates that the flow is governed by the following dimensionless parameters.

$A_1 = h/d$	Aspect ratio
$A_2 = h/l$	Aspect ratio
$Pr = \nu / \kappa$	Prandtl number
$Ra = g \alpha \Delta T \ h^3 / \nu \kappa$	Rayleigh number
$Ma = \gamma_T \ \Delta T \ l \ / \mu \kappa$	Marangoni number
$Ca = \gamma_T \ \Delta T / \gamma$	Capillary number
θ	Contact angle

The notation is standard. Since our interest will be in experiments performed with fixed aspect ratios and fixed fluid, with varying ΔT, an equivalent parameterization is to consider the Marangoni number and the ratio of Ra to Ma as the independent dynamic groups. Thus we define

$$G = Ra/(Ma\ A_1) = \rho g \alpha \ h^2 / \gamma_T$$

The group G has been discussed in many contexts, but no uniform convention exists regarding its name. Its numerical value gives an indication of the relative importance of buoyancy to thermocapillarity, and it has the advantage of being independent of the applied temperature difference.

In contrast to the fairly extensive studies of other cavity flows, our understanding of thermocapillary cavity flow remains primitive. Simple parallel flow solutions with conductive temperature profiles that presumably apply for low aspect ratio and low Prandtl number may be easily obtained. Numerical analysis of strongly convective thermocapillary flows by Zebib et al(1985) and Carpenter & Homsy(1988a) in a cavity of unit aspect ratio has established that, in the limit of large Marangoni number, a finite temperature gradient remains over the entire free surface. This in turn leads to a global flow structure that is qualitatively identical to that of the driven cavity, i.e. a central thermocapillary vortex of constant vorticity and constant

temperature, adjacent to viscous, heat conducting boundary layers near the free and no-slip boundaries of the cavity. This structure is robust, and occurs as Ma -> ∞ , regardless of the Prandtl number, although the evolution of the structure as Ma is increased is highly Prandtl number dependent, Carpenter & Homsy(1988a).

It is natural to also enquire into the structure of two-dimensional thermocapillary-buoyancy driven flow, referred to hereafter as "combined convection", since the two distinct limits of a Gill-type structure on the one hand, and the Prandtl-Batchelor structure on the other are so different. Some preliminary numerical work on combined convection was reported by Bergman and Ramadhyani(1986). This issue is addressed in detail in the computational study of Carpenter & Homsy(1988b), in which it is concluded that thermocapillarity dominates all such cavity problems, in the limit of fixed ratio of Rayleigh to Marangoni numbers, as either one tends to infinity. The reason for this somewhat unanticipated result is that the thermocapillary boundary layer near the free surface is thicker, in an asymptotic sense, than the buoyancy layers on the vertical walls, and thus provides the dominant source of vorticity driving the motion.

Very little is known about stability and transition in such cavity flows; see the recent review by Davis(1987). Smith and Davis(1983a,1983b), have analyzed the linear stability of simple base state velocity profiles corresponding to conductive base states, with the result that either two- or three- dimensional modes of instability can be present, dependent upon the Prandtl number.

Experimental studies of either thermocapillary convection or combined convection in a cavity are few, and are almost entirely limited to regimes of aspect ratio and/or Prandtl numbers for which conduction dominates; Kirdyashkin(1984). Recently, Lamprecht et al(1988) have reported a study of both pure TC and combined convection in a cavity of roughly cubical geometry. The pure TC results, which included both flow visualization and velocimetry taken from streak photographs, were obtained in the microgravity enviornment of the US Space Shuttle. Although the results are influenced to a large degree by surface contamination, the qualitative structure at extremely high Marangoni numbers Ma=4.6×10^5 is appropriate to a Prandtl-Batchelor flow as computed by Zebib et.al. Their results on combined convection illustrate the competition between the Gill and Prandtl-Batchelor structures, showing clear evidence of a thermocapillary vortex near the free surface that does not easily penetrate the core of the cavity due to the stable vertical stratification obtaining there. We shall have reason to return to a detailed discussion of these results in a later section.

A number of experimental studies of TC convection in cylindrical capillary bridges suspended between differentially heated cylinders have been reported by Schwabe and co-workers(1981a,b) and by Kamotani et al(1984), using fluids of Pr approximately 10. These studies have shown that the steady, axisymmeteric toroidal thermocapillary vortex first becomes unstable to a non-axisymmetric time-periodic precession of the axis of the vortex. While many experimental data have been accumulated regarding the dependence of the critical Ma as a function of aspect ratio, Capillary number, etc., understanding of the mechanism of the instability remains elusive.

Thus we find that, in spite of the central role cavity flows play in other contexts, they have not been well-investigated in the case of combined convection. Little experimental evidence about the flow structure, instability points, and post-instability behavior is available. Much of our knowledge about the two dimensional flow is obtained through numerical analysis.In these studies, assumptions are made regarding contact line behavior, ranges of values of contact angles, and the importance of free surface deformation, and results are limited by numerical resolution to moderately large values of Ma, Ma = 10^5, and to limited ranges of the other parameters. Our interest in this work is to make some basic observations and quantitative measurements of this general class of flows, and to compare these with what is known from analytical and numerical studies.

We recognize at the outset that the problem is one governed by at the minimum, five independent dimensionless groups, and a complete parameter study is obviously out of the range of a single study. We also anticipate from what is known from the study of other cavity problems, that the range of phenomena, especially with regard to the possible modes of instabiltiy, can be quite rich. Since so little was known when we began this work, we decided to limit the present investigation to one cell, to one working fluid, and to one dimensional depth of the fluid in the cell. Thus the two aspect ratios, the Prandtl number, and the group G are all held fixed in this investigation. As will be seen, no attempt was made to control or modify the contact angle. Thus, the main experimental variable is the imposed temperature difference. We choose to report the results in terms of the Marangoni number, Ma, but this is an arbitrary choice, as any two of Ma, Ra, and G specify the dynamical parameters.

2. Apparatus and Procedure

The convective motions are established in a spectrophotometer cell comprised of five optical windows, with a square cross-section 1cm x 1cm and 3.8 cm in length. Plexiglass baths are glued on each vertical side wall. Water at constant temperature is pumped from two thermostatically controlled tanks, through the side baths, thus allowing a temperature difference ΔT to be maintained across the cavity to within an accuracy of $\pm$ .1°C. The hot and cold temperatures were adjusted so that the mean temperature in the cavity was always close to room temperature. In this way, we hoped to minimize heat losses from the top, bottom, and end walls. Small pieces of insulating material were placed on the end walls as well, and were removed only for the short time taken to photograph the motion. The cell is set on an optical translation stage to allow a study of the convective motion along the third dimension of the cell. There is a hole in the translation stage to allow for the passage of the laser illumination, and to minimize back reflections.

The working fluid used is a silicone oil with a viscosity of 0.65 cSt; its physical properties are tabulated in the table 1. This table also presents the temperature dependence of the Prandtl number in the range of temperature used. This dependence is almost entirely due to the temperature dependence of the viscosity, but over the range of temperatures studied, the Prandtl number varied by 10% at most.

Flow visualization and velocimetry were accomplished by a laser technique. The Particle Image Velocimetry (PIV) has been developed to measure quantitative velocity data for fluids flows, see e.g. Lourenco & Krothapali (1987), Adrian (1986) and the recent review by Hesselink(1988).

A laser beam from an Argon laser (2W at 514.5nm) is focused with a system of cylindrical and spherical lenses on a plane to form a light sheet, as shown in Figure 2. The laser sheet, 0.5mm x 12mm , illuminates a chosen section in the cell. The laser is modulated using a chopper (or sector) model SR 540 from Stanford Research Systems Inc. Palo Alto, providing pulses of light with adjustable frequency. The chopping frequency is dependent on the range of velocities present, which in turn depends upon the Marangoni number and the spatial location within the cavity. In our experiments, the chopping frequency was varied from 4 to 40Hz. In the technique, a negative is multiply exposed; the total exposure time, Δt, determines the number of exposures taken on the same picture i.e. the number of spots given by the same tracer. The exposure time used was dependent not only on the Marangoni number of the experiment, but also the spatial region of the flow that was to be investigated, and the optimum time was determined by trial and error.

Both velocimetry and flow visualization are accomplished by light scattered by seeding particles in the illuminated plane. The assumption in such techniques is that the seed particles follow the fluid without significant lag and do not alter the flow dynamics. The first requirement limits the size particles, the second limits the particle concentration. Spherical polystyrene particles of 7μm diameter have been used at a volume concentration of 10^{-2}. Under these conditions of low seeding concentration, the image pattern consists of sequence of superimposed particle images. This image is recorded by means of a camera, with unit magnification, on a high resolution film (Kodak technical pan 2415, ASA 75, with a resolution of about 300 lines-pairs/mm).

Flow visualization consisted of a sequence of such multiply-exposed photographs, as either the Marangoni number or the axial plane was varied. In velocimetry, the local fluid velocity is derived from the ratio of measured spacing between the images produced by the same tracers and the time between exposures or pulses of light. The recorded image is a complicated random pattern. One of the methods of analysis is to produce Young's fringes by local coherent illumination of the multiple exposed photographic film, as shown schematically in Figure 3. Figure 4 shows an example of a photograph and corresponding fringe patterns, produced by interrogation of the photographic negative by a second small Ne-He laser. These fringes have an orientation perpendicular to the direction of the local displacement vector and a spacing inversely proportional to its magnitude.

In order to validate the experimental set-up and the velocimetry technique, experiments on the pure buoyancy convection problem were performed by simply eliminating the free surface. This problem has been extensively studied, and is now well-understood; for an aspect ratio $A_1=1$, the works of Simpkins & Dudderar(1981) and of Elder(1965), have shown that the primary flow field is a single cell with entrainment and detrainment of the flow in the vertical buoyancy boundary layers. At Rayleigh numbers on the order of 10^6, secondary flows consisting of weak circulations attached to the vertical layers appear. In the boundary layer limit for large Ra, the vertical velocity scales as $\Delta T^{1/2}$.

This problem was investigated using the cell and techniques described above. First, flow visualization revealed the expected secondary rolls along the vertical boundaries at a value of Ra = $5x10^6$. A sequence of photographs taken along the cell length at different values of Ra allowed us to verify that the flow is two-dimensional. This verification is important, as it pertains to our discovery of three-dimensional flows, described in the next section. As a quantitative check, the vertical velocity measured by particle image velocimetry at a chosen point within the boundary layer at the horizontal midplane was found to scale with $\Delta T^{1/2}$. Thus, this first sequence of experiments showed that the set-up is both qualitatively and quantitatively accurate.

Our experiments covered the following range of parameters. The depth of fluid is set at a level h = 0.68 cm. The width of the cell is 1 cm and its length, 3.8 cm. In what follows the recorded positions are made dimensionless with the relevant dimension, so that all coordinates range from zero to one. No attempt was made to control the contact angle at a value other than that naturally occuring for silicone oil on glass, which we estimate to be approximately 53 degrees. Thus the meniscus is curved in the static rest state, and remains so under conditions of flow. The capillary number, a measure of the degree of surface deformation as a result of dynamic normal stresses was at most 0.1, and no appreciable surface deflection or change in the contact angle was noted. As mentioned in the introduction, the imposed temperature difference is the primary experimental variable, with all the others parameters fixed at the following values: $A_1 = 0.68$, $A_2 = 0.18$, $Pr = 8.4$, $G = 2.5$. We report the results in terms of the Marangoni number, Ma.

The procedure followed was to disperse the particles in the fuid by agitation, establish the desired ΔT, establish a steady state, and then take the desired data. In general, the fluid motion is steady approximatly 0.5h after a change in conditions, and steady-state conditions have been established for periods as long as 4 hours. In some cases, axial sections of the flow were taken by moving the cell on the translation stage relative to the optics, which remained fixed. In other cases, a sequence of photographs were taken at fixed axial location for varying temperature difference. Temperature sequencing was done by both increasing and decreasing ΔT, allowing us to observe any hysteresis present.

3. Results

The temperature differences covered in this work ranged over almost two orders of magnitude, from 0.3 to 20 ^{o}C. The corresponding range of Ma and Ra covered are given in Table 2. In addition to qualitative and quantitative details, the main result of this work is that we have discovered and identified a transition from two dimensional to three dimensional convection, which for the parameters of the experiment, occurs at a specific value of the Marangoni number. For convenience, we will separate the discussion into two parts, dealing with two- and three-dimensional flows respectively.

3(a) Two Dimensional Flows

Figure 5 shows a sequence of visualizations taken at fixed location, y=0.31, with varying Ma : 6.3×10^3, 4.3×10^4, 1.1×10^5. In the photographs the cold wall is on the right and the hot wall on the left. The common feature of these pictures is a unicellular cell, with strong velocities along the free surface toward the cold corner (right) and a weaker reverse motion in the bottom part of the

cell toward the hot wall. Between these two layers exits a core region where there is little detectable motion. As the value of Ma increases, the top thermocapillary boundary layer becomes thinner, the lower part of the cell presents a more visible detrainment of the flow near the lower cold wall. We interpret this behavior as being due to the development of some stable vertical stratification in the lower regions of the cavity. With increasing Ma, the fluid circulation intensifies with the average flow velocity in the cell increasing, as expected. Notice that for Ma = 1.1×10^5, the reverse motion from the cold to the hot wall, has apparently split in two circulations; one in the upper part, where the motion is associated with a thermocapillary vortex, and a lower one where the flow follows the cell bottom.

Velocity profiles

The local horizontal velocity is measured from each photograph at the vertical mid-plane of the cell (x=0.5, y=0.31), for different heights in the liquid ($0< z< 1$). Velocity profiles obtained by interpolation of these data are presented Figure 6. They show features typical of surface tension driven flow, namely a large free surface velocity, and a core region of weak recirculation. Although the parameter values in these studies do not allow a direct comparison, these velocity profile in Figure 6b is in qualitative agreement with those calculated by Zebib, Homsy &Meiburg (1985) for the case of pure thermocapillary convection, and by Carpenter & Homsy(1988b) for combined convection. As ΔT increases, the velocity in the surface boundary layer increases strongly, the vortex shifts near the free surface and we can observe the splitting of the back flow into a current that follows the wall, and another that rejoins the thermocapillary vortex near the surface, as before.

Axial Sectioning

In addition to this series of measurements which consisted of flow visualizations and velocimetry in a fixed plane with varying Ma, it is also possible to interogate the flow along the cell length at various values of y ($0.18<y<0.9$) for fixed Ma. In this range of ΔT, the visualizations are identical to one to another, leading to the conclustion that the fluid flow is two-dimensional for Ma below 1.1×10^5. This conclusion is supported by a quantitative analysis of the velocity profiles, as discussed below.

3(b) Three Dimensional Flow

As we have indicated several times, the flow is not always two dimensional, and in fact we have observed a transition from the typical two dimensional flow shown, for example, in Figure 5a, to a three-dimensional one of much more complicated flow structure.

Flow Visualizaton

Figure 7 shows flow visualizations taken at y=0.31 for ΔT of 7, 15.5 and 20°C, corresponding to Ma of $1.5x10^5$, $3.25x10^5$, $5x10^5$ respectively. Again, we observe the same qualitative flow characteristics as before. The maximum flow velocity is observed in the free surface. For a $\Delta T>15.5$°C, we note the existence of two adjacent vortices rotating in the same sense just below the surface with the appearance of an apparent saddle point in the flow. This pair of vortices is more obvious for $\Delta T=20\ ^oC$, Ma = 5×10^5, the highest Marangoni number studied. As the value of Ma is increased, the vortex center is shifted near the surface, the thicknesses of the layers around it decrease and a region of very slow motion appears between the two backflow layers. We shall see that these features, while they do not exclude the flow from being two-dimensional, are characteristic of three dimensional flow.

Velocity profiles

Figure 8 presents the velocity profiles obtained at x=0.5, y=0.31, corresponding to the pictures in Figure 7. All the phenomena observed in the precedent range of Ma are amplified here : both the surface velocity and its gradient in the z-direction are large and the two streams of backflow are prominent. It is possible to point out the transition from two to three dimensional flow by vertical integration of the horizontal velocity profiles, which yields a measure of the mass flux into or out of the x-z plane. If the motion is two dimensional this mass flux should be zero. Results of such calculations for profiles at the midplane of the cavity are shown on Figure 9, and they indicate that the flow is definitely three-dimensional for $Ma>1.5x10^5$. Similar analyses of the velocity profiles at horizontal positions other than the midplane yielded similar results, with the value of the net mass flux being a function of the chosen plane whenever the flow was three-dimensional, as expected.

Axial Sectioning

Visualizations taken at different axial positions in the cell show a flow pattern which clearly varies with distance, providing definitive evidence for three-dimensional flow. This difference in visualizations first appears for $\Delta T = 7\ ^{o}C$, or $Ma = 1.5x10^5$. As we will see, the three-dimensionality becomes stronger at higher Ma, but this is the lowest value for which the flow is unambiguously three-dimensional, and therefore represents our best estimate of the critical Marangoni number for transition, at these values of the other parameters.

The transition to a 3D flow and the amplitude of the pertubations it induces on the plane flow can be also observed by plotting the vortex center position as a function of x versus the y value of the picture, as shown Figure 10 for various values of ΔT. As can be seen, for Ma less than $1.1x10^5$, the curve is flat, the vortex center has the same position all along the cell. For $Ma = 1.1x10^5$, a 3D effect appears, but is localized near the ends of the cell, with the motion in the center region of the cell ($0.3 < y < 0.7$) still essentially two dimensional.

The 3D flow is fully established for $Ma >= 3.25x10^5$; it exhibits a symmetry about the midplane and an axial periodicity along the y-direction. Note that the curves indicate that the first departures from two dimensional flow occur near the end walls of the cell. Indications are clear, especially at high Ma, that the three dimensional motion is periodic in the axial direction. We made studies in which we investigated the reproducibility of these results. These experiments were done by bringing the system to a given Ma from a state of rest, and measuring the resulting convection in the manner described above. In all cases, the convection was identical, indicating that the instability is characteristic of a supercritical bifurcations. However, in many cases,we observed a difference in the axial phase angle of the convection. The two curves labeled (2) and (3) in Figure10 B are a good example of this.

At the highest Marangoni number studied, $\Delta T=20°C$, $Ma=5*10^5$, the axial periodicity of the flow is most pronounced. On examining visualizations taken at increasing y value, we can observe that, whereas the flow in the bottom regions of the cavity does not vary substantially with axial position, the features of the top thermocapillary eddy do. Figure 11 shows a sequence of such visualizations. In the surface layer, we notice first (a) the existence of two clockwise vortices, side by side, which then evolve into an elongated vortex in the central part of the cell (b), which itself splits in two vortices on the next picture (c). This sequence, two vortices then one central vortex and then two vortices again, repeats itself all along the container, so that (b) is identical to (d) & (f). As mentioned earlier the flow is symmetric about the cell midplane y=0.5.

In order to probe the structure of the flow in the axial direction, the laser was reoriented to illuminate the flow in the y-z plane, along the center of the cell, with photographs taken through the water bath normal to the light direction. A good idea of this flow structure is given by a composite visualization, Figure 12. It reveals the existence of a periodic sequence of cardioic convective cells, particles flowing up between the 'hearts' and down inside each 'heart'. The periodicity of the motion inferred from a sequence of front views, are confirmed here by the side views. Four identical patterns are established in the 3.8 cm length, involving a wavelength of 0.95cm. It is of interest to note that these three dimensional structures have a natural tendency to be cubical, i.e. the axial wavelength is comparable to the depth and breadth of the cell, at least for these values of the parameters.

5-DISCUSSION AND CONCLUSION

From a variety of qualitative and quantitative observations and measurements, we are able to conclude that, for the range of parameters studied, combined convection in a cavity undergoes a transition from two- to three-dimensional flow at Ma $=1.5 \times 10^5$. The three-dimensional flow structure is probed and found to consist of a spatially periodic array of cardoic vortices, having an approximately cubical structure. The details of the establishment of this structure is typical of an imperfect bifurcation, probably related to finite cell length or thermal effects at the end walls of the cell. No hysteresis in the transition was observed; however the location of the cardoic cells relative to the fixed end walls varied, suggesting that the phase of the three dimensional flow relative to these walls is indeterminate. These observations suggest, but do not prove, that the observed transition is a supercritical bifurcation. The fact that the cardoic pattern always develops from the end walls suggests that the experiments are characteristic of a perturbed bifurcation, due to modification of the two dimensional flow by the no slip end walls, heat loss out the end wall, or both.

These observations are, to our knowledge, unique, in the sense that such transitions have never been observed before for thermocapillary convection. It is of interest to compare the structure of the flow, as visualized in the x-z plane, with the observations of Lamprecht et al (1988), who conducted a similar experiment in a cell that was roughly cubical. Their visualizations, for G = 35.8, Ma $=5 \times 10^5$, Pr = 49, while not at exactly the same range of parameters, show a structure remarkably similar to that in Figure 11c; see their Figures 4 &5. Although they state the flow was two dimensional, no quantitative evidence was given to support that statement, and, given the fact that the Marangoni number in their experiments was so high, and the cell was roughly

cubical, we speculate that the flow observed by them was roughly identical in structure to one of the cardoic cells observed here.

It remains to speculate on the mechanism of the instability. As mentioned in the introduction, much study has been devoted to the transition between two-dimensional single and multi-cellular convection in buoyancy driven cavity flows of either high or low aspect ratio, and transitions from steady to time dependent two dimensional flow in the case of low Prandtl number convection in unit aspect ratio cavities. While it is not possible to rule out any of the mechanisms operative in these cases, they are not likely candidates, since the structure of the flow that replaces the steady two-dimensional flow in all these examples is not similar to that observed here.

Transition from two- to three-dimensional steady convection has been studied extensively in the case of Rayleigh-Benard convection, in which the "skewed varicose" instability leads to convection rolls with spatially periodic structure, Busse(1978), Azouni (1981). Since our experiments were not devoid of the influence of buoyancy, a mechanism similar to that occuring in Rayleigh Benard convection, and only loosely associated with the fact that the flow is driven by thermocapillarity, remains a possiblility. Another possibility is related to the structure of the basic two dimensional flow. As noted in the introduction, the boundary layer structure of combined convection, taken as the limit of Ma -> ∞, G fixed, is identical to the pure thermocapillary flow problem, i.e. a Prandtl-Batchelor eddy of constant temperature and vorticity, Carpenter & Homsy(1988b). It is therefore possible that the instability observed here is related to that observed in driven cavity flows. While the mechanism of instability in the driven cavity remains unexplained at present, the speculation of Koseff and Street (1984a,b) that it is associated with the centrifugal Taylor-Gortler instability of the primary vortex cannot be ruled out in the present case. A last possiblity, that the mechanism is intrinsically related to the thermocapillary stress at the surface, remains a third possibility. These issues are under current study.

Acknowledgement We wish to acknowledge support of this work through a ESA postdoctoral fellowship to Pascale Gillon, and a NASA Microgravity Science Grant to G.M. Homsy. We are thankful to Prof.D. Schwabe for sending us a copy of Lamprecht et al. before its publication.

References

ADRIAN, R. J. 1986 *Proc.Third Int.Symp. Applications of Laser Anemometry to Fluids Mechanics,* Lisbon.

AZOUNI, M. A. 1981 *Physico Chemical Hydrodyn.* **2**, 295.

BERGMAN,T. L. & RAMADHYANI 1986 *Numerical Heat Trans.* **9**, 441.

BUSSE, E. H. 1978 *Rep. Prog. Phys.* **41**, 1929.

CARPENTER, B. M. & HOMSY, G. M. 1988a High Marangoni Number Convection in a Square Cavity, part 2 *Phys. Fluids* (submitted).

CARPENTER, B. M. & HOMSY, G. M. 1988b Combined Buoyant-Thermocapillary Flow in a Cavity *J. Fluid Mech.* (submitted).

DAVIS, S. H. 1987 *Ann. Rev. Fluid Mech.* **19**, 403.

DRUMMOND, J. E. & KORPELA, S. A. 1987 *J. Fluid Mech.* **182**, 543.

ELDER, J. W. 1965 *J. Fluid Mech.* **23**, 77.

GHIA, U., GHIA, K. N. & SHIN, C.T. 1982 *J. Comp. Phys.* **48**, 387.

GILL, A. E. 1966 *J. Fluid Mech.* **26**, 515.

HART, J. 1971 *J. Fluid Mech.* **47**, 547.

HART, J. 1972 *J. Atmos. Sci.* **29**, 687.

HESSELINK, L. 1988 *Ann. Rev. Fluid Mech.* **20**, 421-85.

KAMOTANI, Y., OSTRACH, S. & VARGAS, M. 1984 *J.Crystal Growth* **66**, 83.

KIM, J. & MOIN, P. 1985 *J. Comp.Phys.* **59**, 308.

KIRDYASHKIN, A. G. 1984 *Int. J. Heat Mass Transfer* **27**,1205.

KOSEFF, J. R. & STREET, R. L. 1984a *Trans. ASME : J. Fluids Eng.* **106**, 385.

KOSEFF, J. R. & STREET, R. L. 1984a *Trans. ASME : J. Fluids Eng.* **106**, 390.

LAMPRECHT, R., SCHWABE, D. & SCHARMANN, A. 1988 Thermocapillarity and Buoyant Convection in an Open Cavity under Normal and Reduced Gravity. *J. Fluid Mech.* (submitted).

LOURENCO, L.M. & KROTHAPALI, A. 1987 *Exp. Fluids* **5**,29.

SCHREIBER, R. & KELLER, H. B. 1983 *J. Comp. Phys.* **49**, 310.

SCHWABE, D. & SCHARMANN, A. 1981a *J. Crystal Growth* **52**, 435.

SCHWABE, D. 1981b *Physico Chemical Hydrodyn.* **2**, 263.

SIMPKINS, P. G. & DUDDERAR, T. D. 1981 *J. Fluid Mech.* **110**, 433.

SMITH, M. K. & DAVIS, S.H. 1983a *J. Fluid Mech.* **132**, 119.

SMITH, M. K. & DAVIS, S.H. 1983b *J. Fluid Mech.* **132**, 145.

WALKER, K. L. & HOMSY, G. M. 1978 *J. Fluid Mech.* **87**, 449.

ZEBIB, A., HOMSY,G. M. & MEIBURG, E. 1985 *Phys. Fluids* **28**, 3467.

Figure Captions

Figure 1. Schematic of the apparatus

Figure 2. Schematic of the optics

Figure 3. Schematic for the interferometric interrogation of negatives

Figure 4. An example of a negative and the resulting fringe pattern from different points in the flow domain. The orientation and spacing of the fringes are related to the velocity vector at a point.

Figure 5. Sequence of flow visualizations at a fixed position, with increasing Ma, (a) $Ma=6.3 \times 10^3$, (b) $Ma=4.3 \times 10^4$, (c) $Ma=1.1 \times 10^5$.

Figure 6. Horizontal velocity profiles at the midplane of the cavity. (a) $Ma = 6.3 \times 10^3$; (b) $Ma = 1.1 \times 10^5$.

Figure 7. Flow visualizations for y=0.38. (a) $Ma = 1.5 \times 10^5$ (b) $Ma = 3.25 \times 10^5$ (c) $Ma = 5 \times 10^5$.

Figure 8. Horizontal velocity profiles at x=0.5, y=0.38 for (a) $Ma = 1.5 \times 10^5$ (c) $Ma = 5 \times 10^5$

Figure 9. Mass flux obtained by integration of the horizontal velocity profiles.

Figure 10. Location of the center of the primary vortex as a function of axial position : (a) varying Ma; (b) replicate experiments at $Ma = 1.5 \times 10^5$

Figure 11. Sequence of streaklines as a function of axial position, $Ma= 5 \times 10^5$; (a) y = 0.19 (b) y = 0.25 (c) y = 0.31 (d) y = 0.375 (e) y = 0.44 (f) y = 0.5.

Figure 12. Composite visualization showing the fully developed structure of the three dimensional flow, taken along the midplane: $Ma = 5 \times 10^5$.

Table 1. Physical properties of Dow Corning silicone oil 0.65 cS.

Table 2. Range of Re and Ma numbers covered during the experiments.

Table 1

$\nu \times 10^{-2}$ $cm^2 s^{-1}$	ρ $g\,cm^3$	$\alpha \times 10^{-3}$ $^{\circ}C^{-1}$	$\kappa \times 10^{-3}$ $cm^2 s^{-1}$	γ $dyne\,cm^{-1}$	γ_T $dyne\,cm^{-1}\,^{\circ}C^{-1}$	Pr 25°C	Pr 13°C	Pr 33°C
0.65	0.758	1.34	0.77	15.9	0.08	8.4	9.5	7.9

Table 2

ΔT °C	0.3	0.8	2.02	5.2	7	10	15.5	20
Ra_{10^4}	1.65	4.2	10.3	27.5	36	52.5	81	105
Ma_{10^3}	6.63	16.8	43	110	147	210	325	420

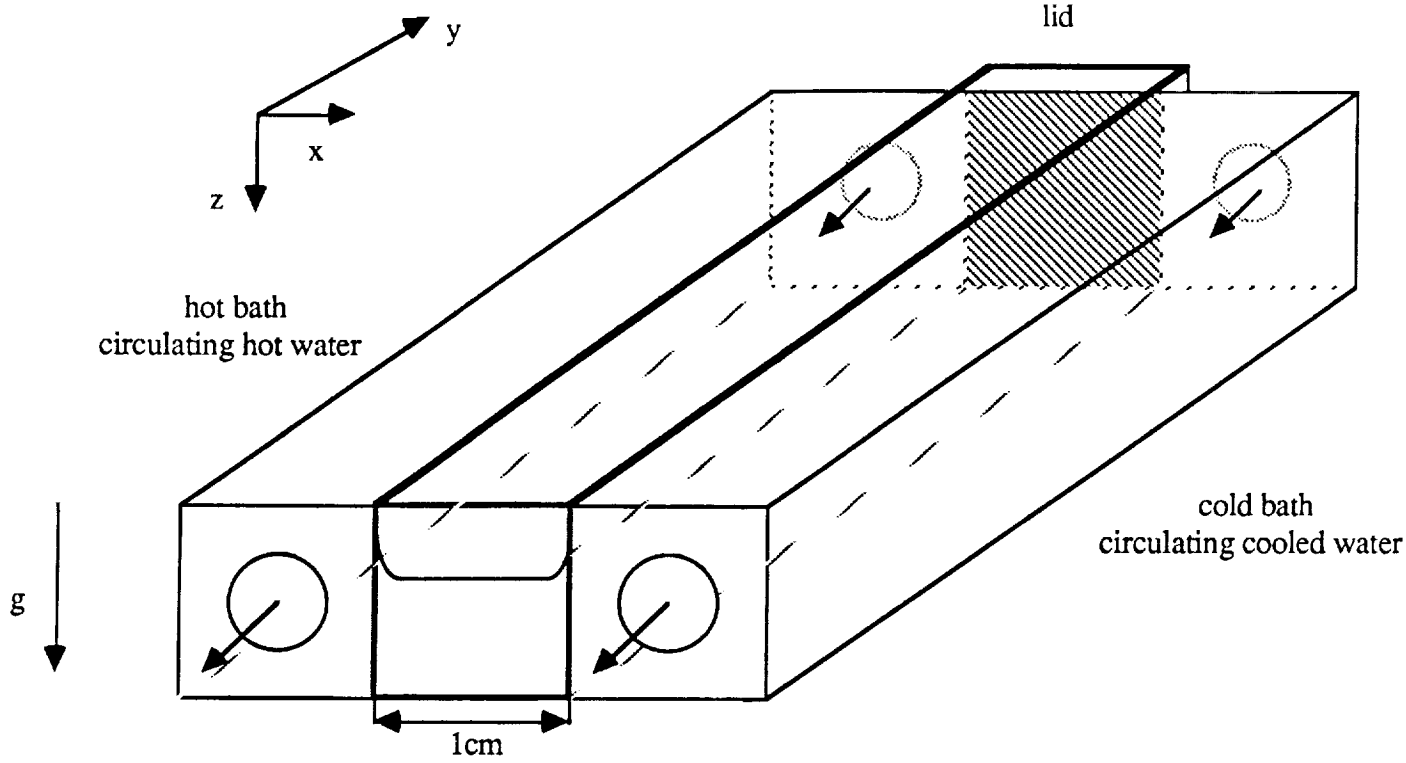
y
x
z
lid
hot bath
circulating hot water
cold bath
circulating cooled water
g
1cm

Figure 1

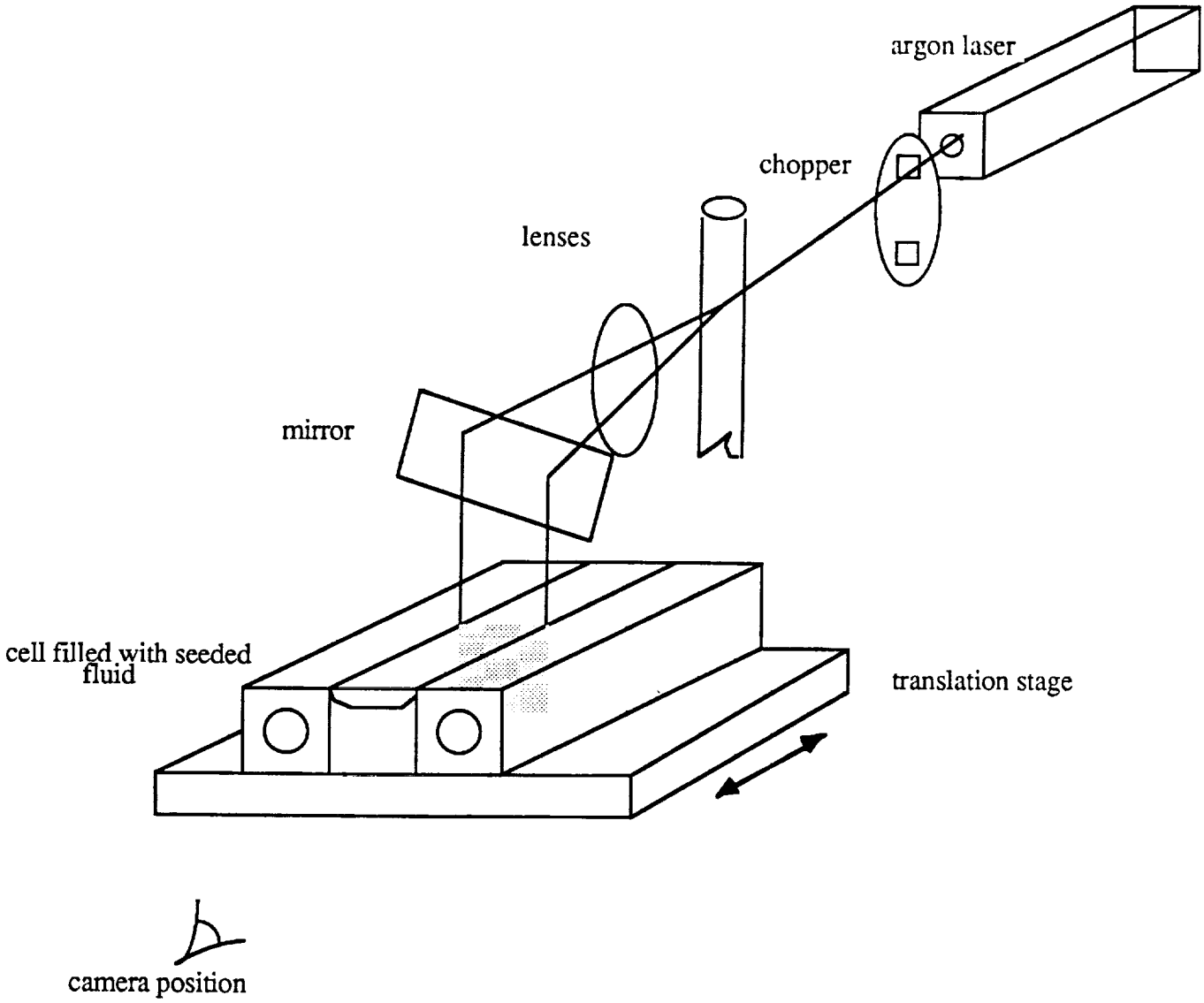
argon laser
chopper
lenses
mirror
cell filled with seeded fluid
translation stage
camera position

Figure 2

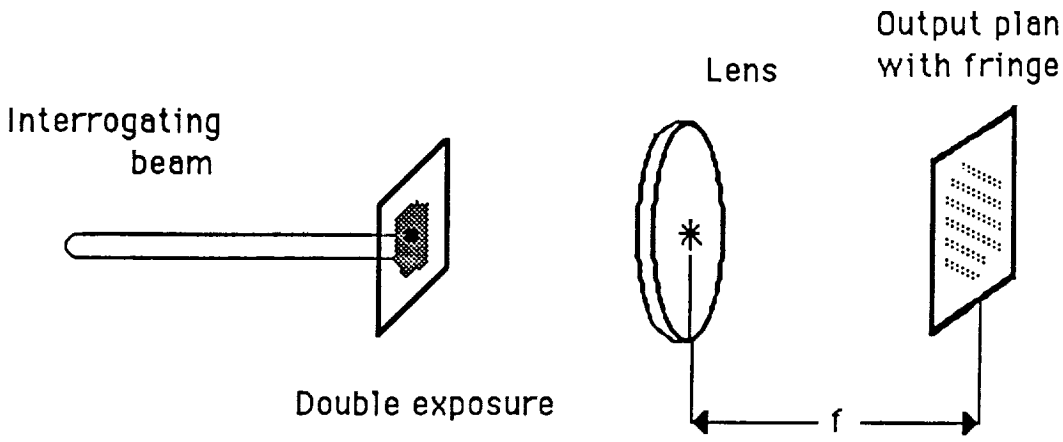
Interrogating
beam
Double exposure
Lens
Output plan
with fringe
f

Figure 3

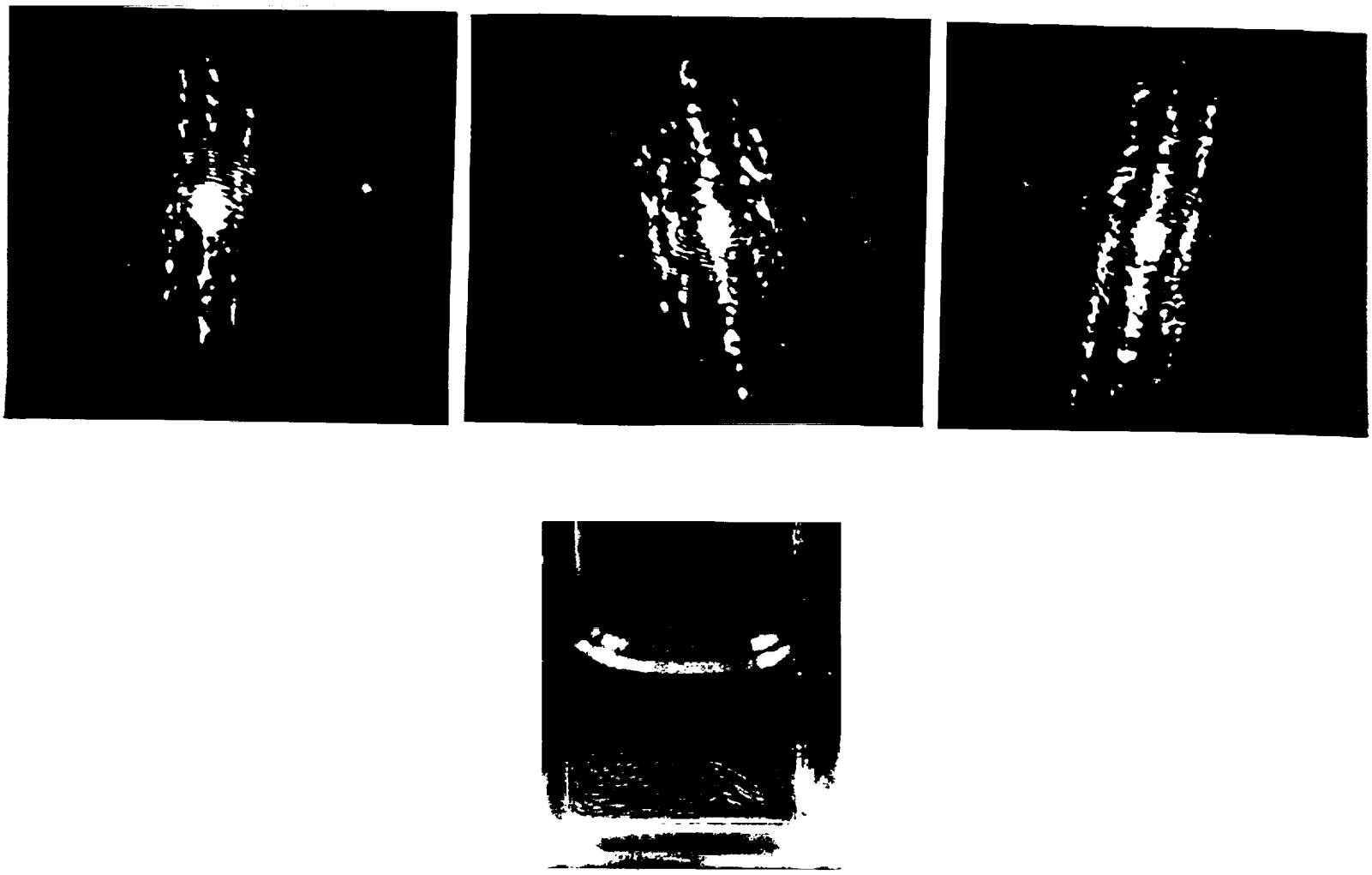

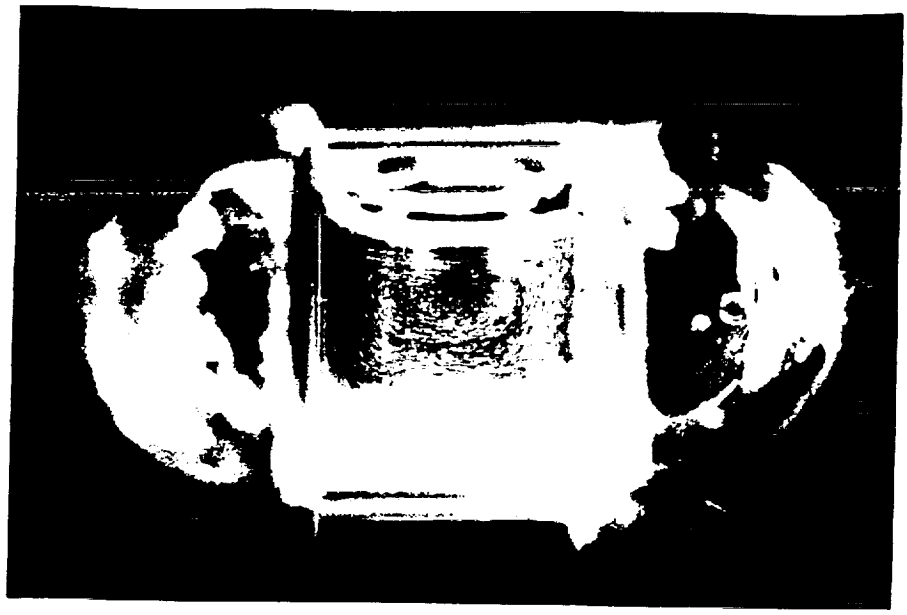

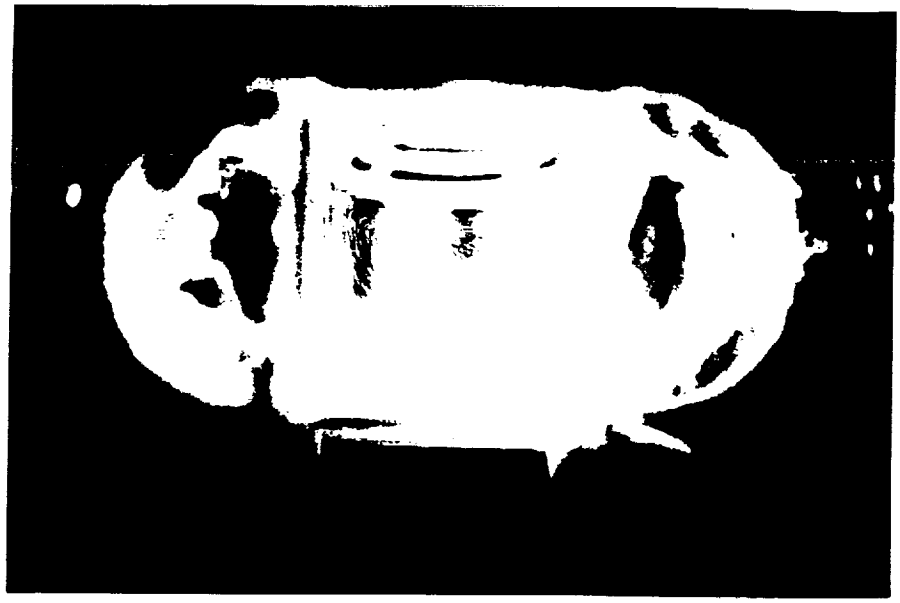

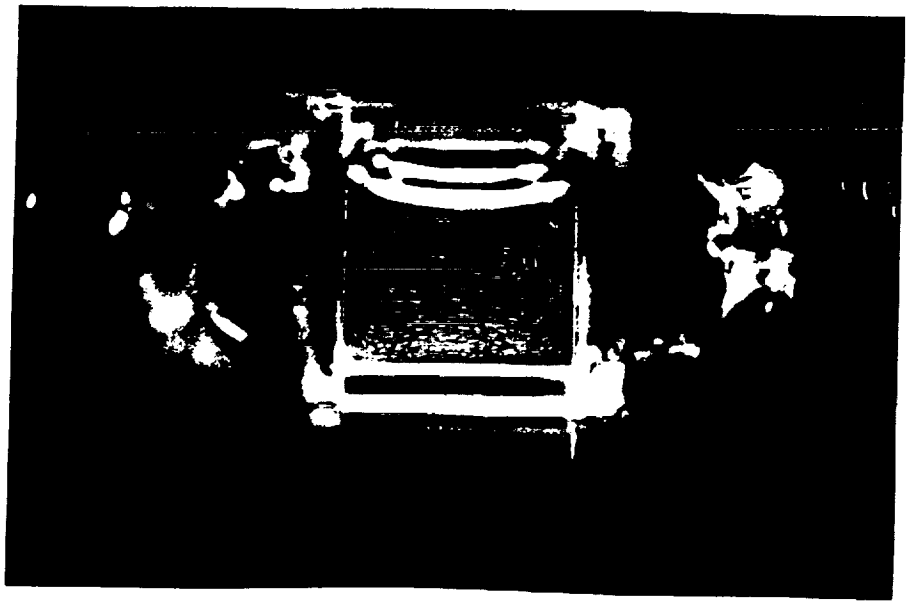

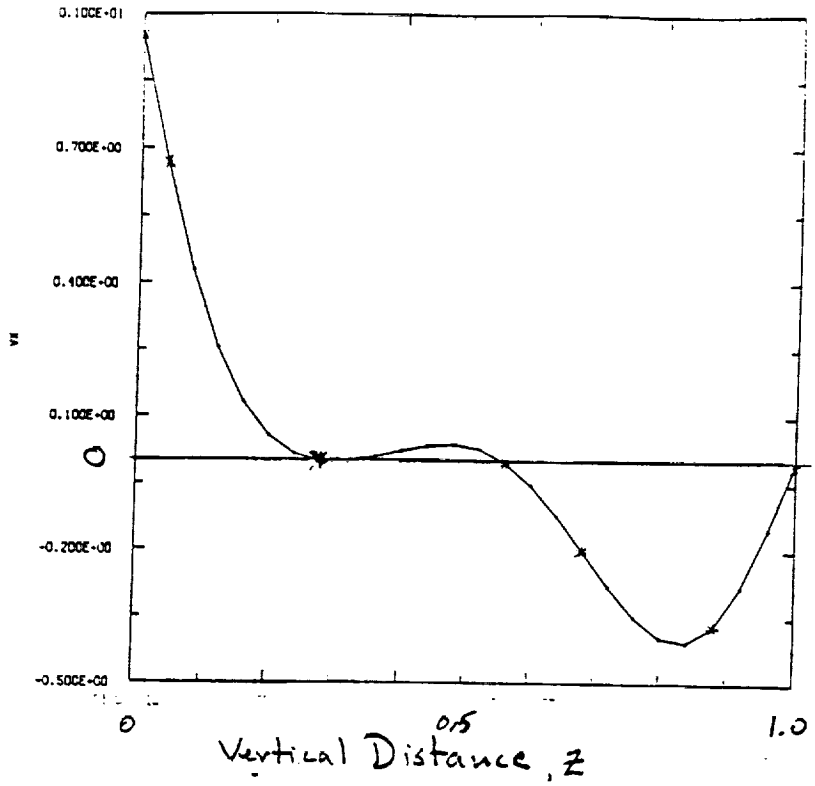

V_x (cm/sec)

(a)

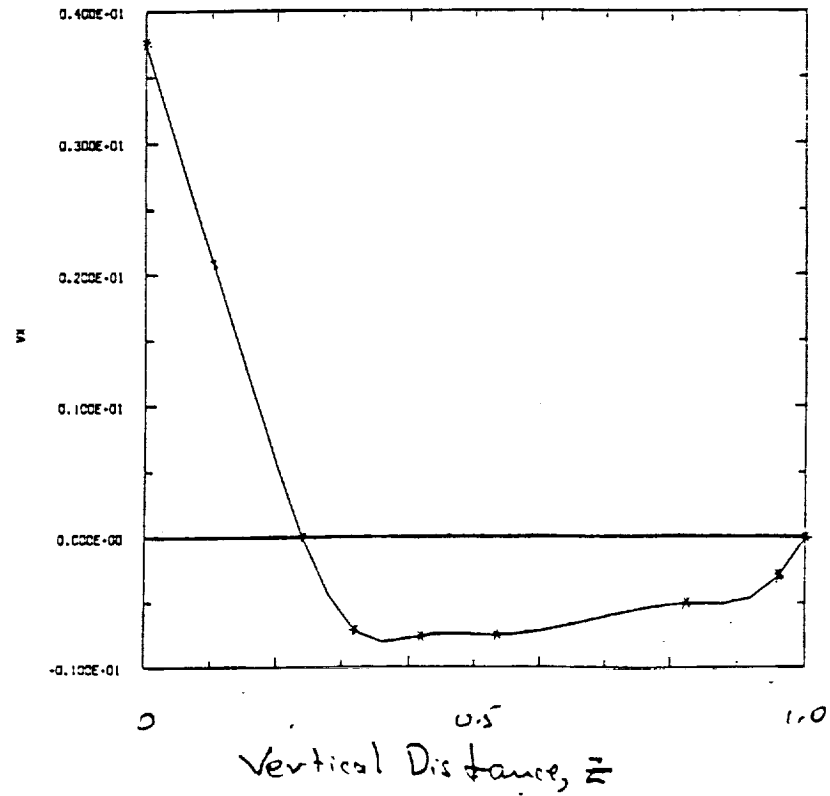

V_x (cm/sec)

(b)

Fig. 6.

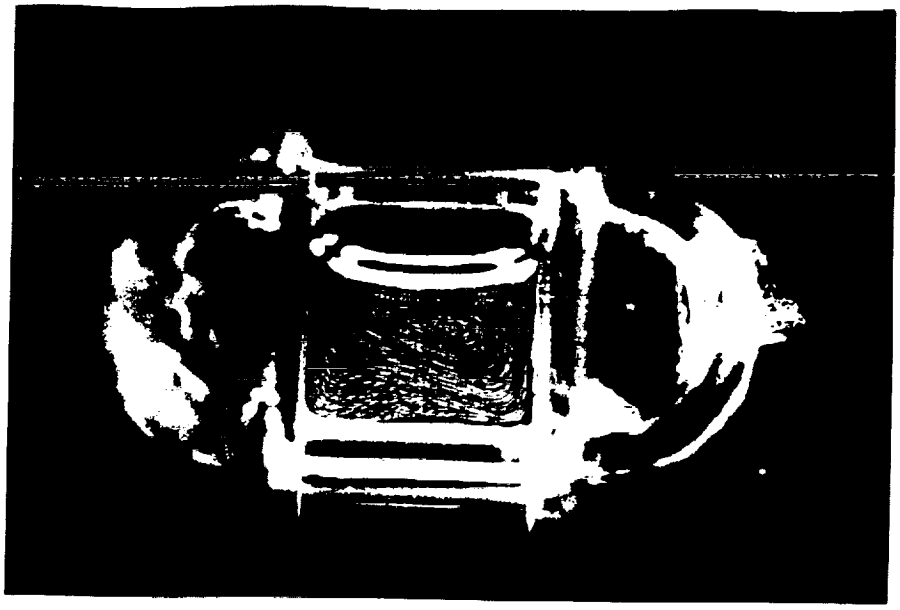

(a)

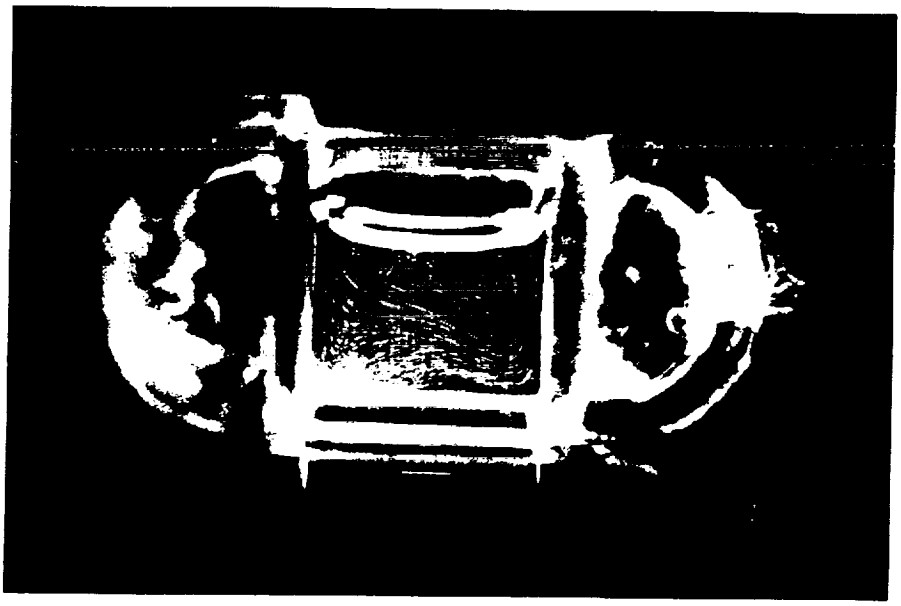

(b)

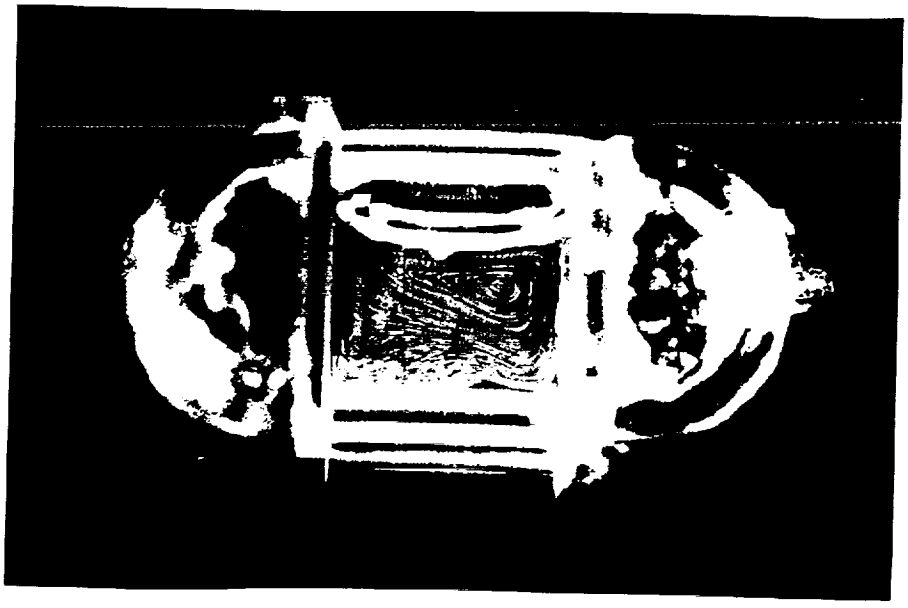

(c)

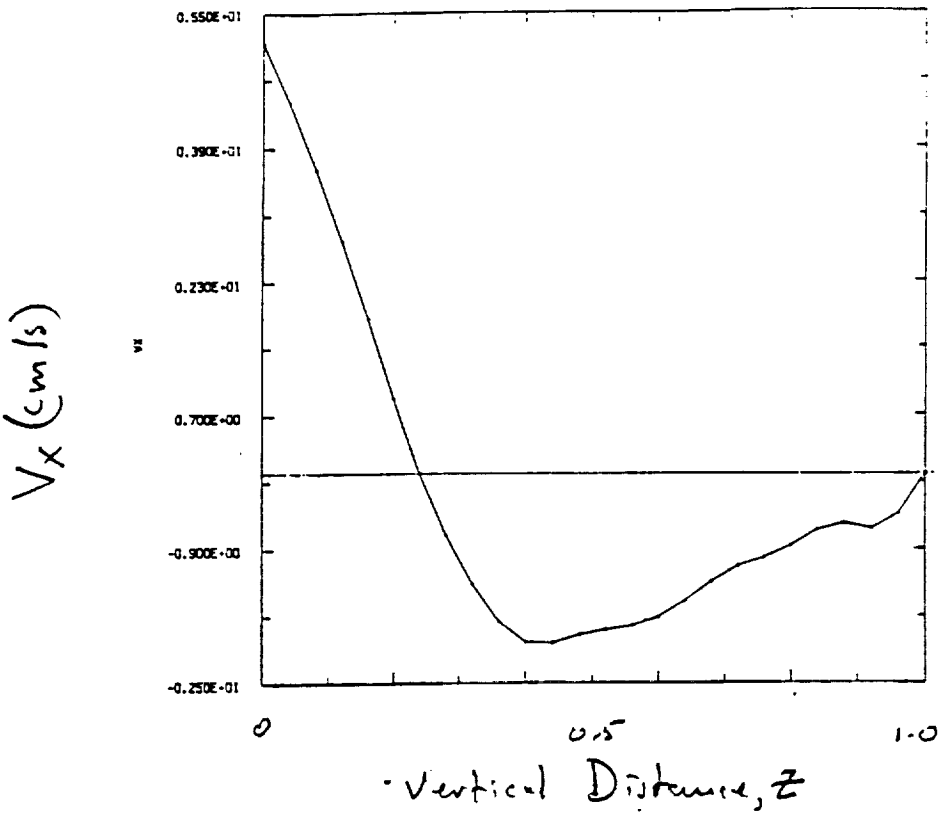

(a)

V_x (cm/s)

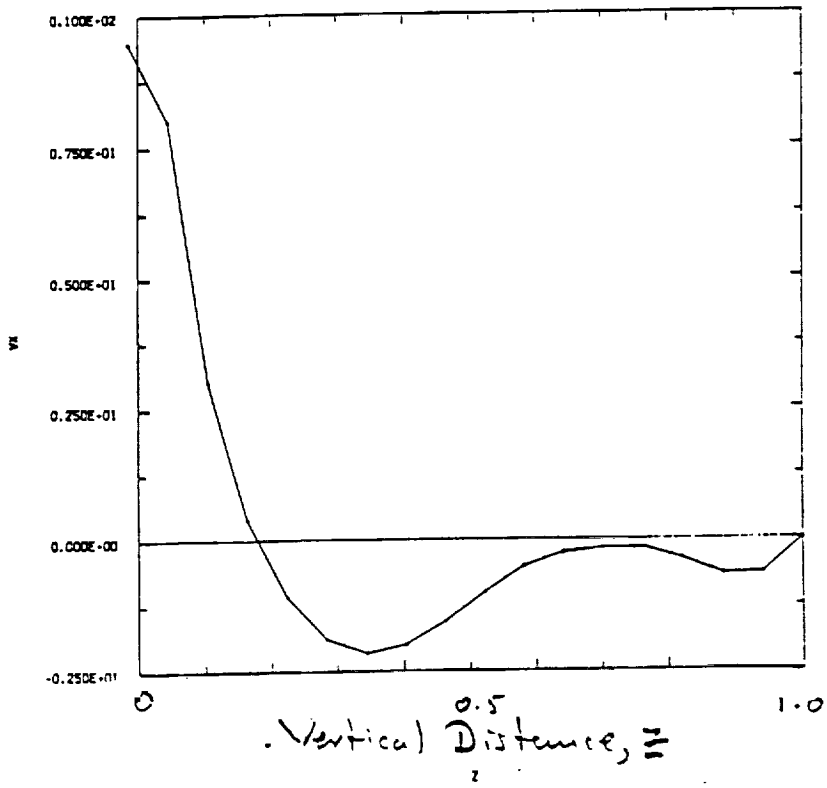

(b)

V_x (cm/s)

Fig 8

Figure 9

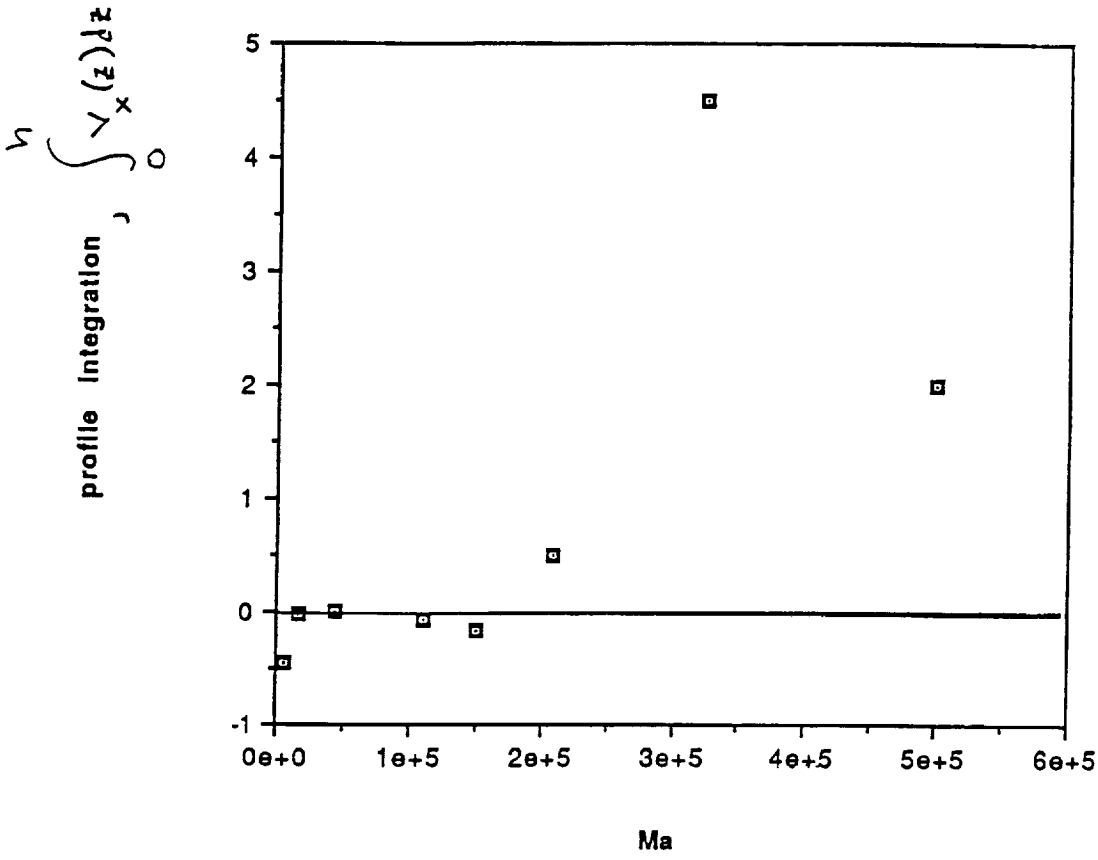
profile integration $\int_0^h v_x(z)\,dz$
5
4
3
2
1
0
-1
0e+0
1e+5
2e+5
3e+5
4e+5
5e+5
6e+5
Ma

Figure 10 (a)

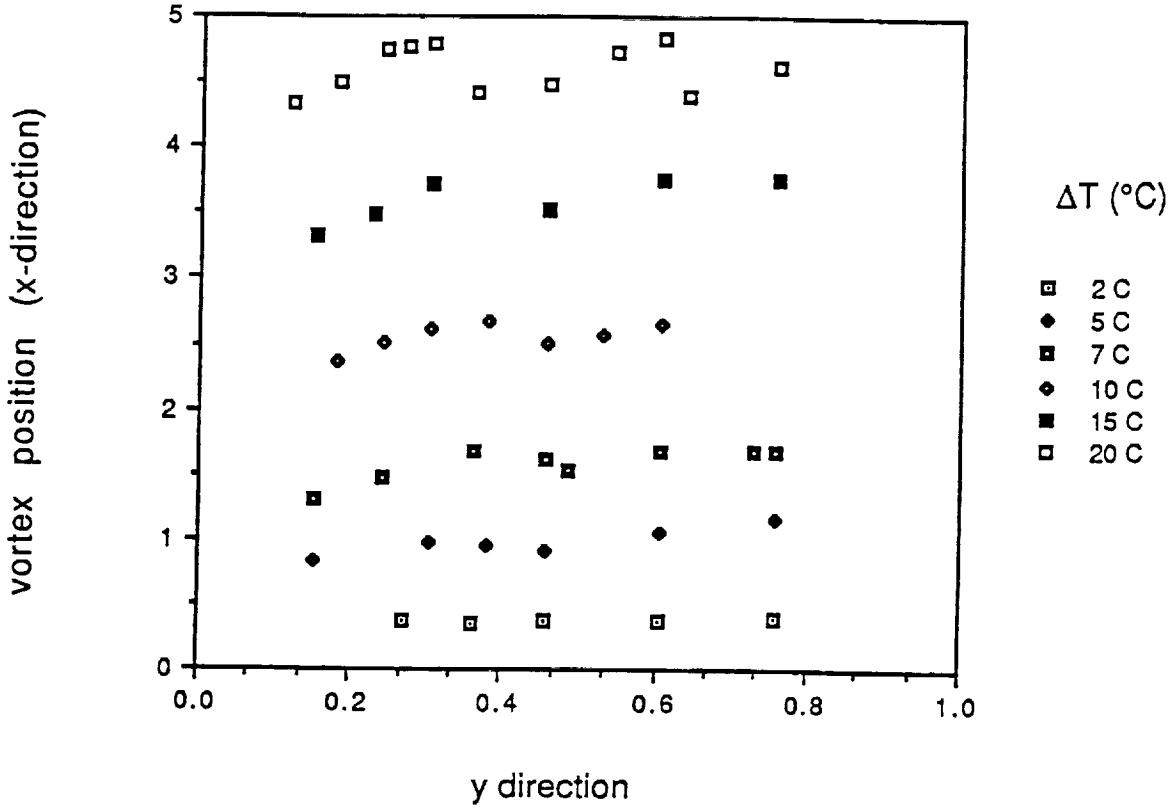

Note: Vortex position shifted vertically by 1 unit for clarity

Figure 10 (b)

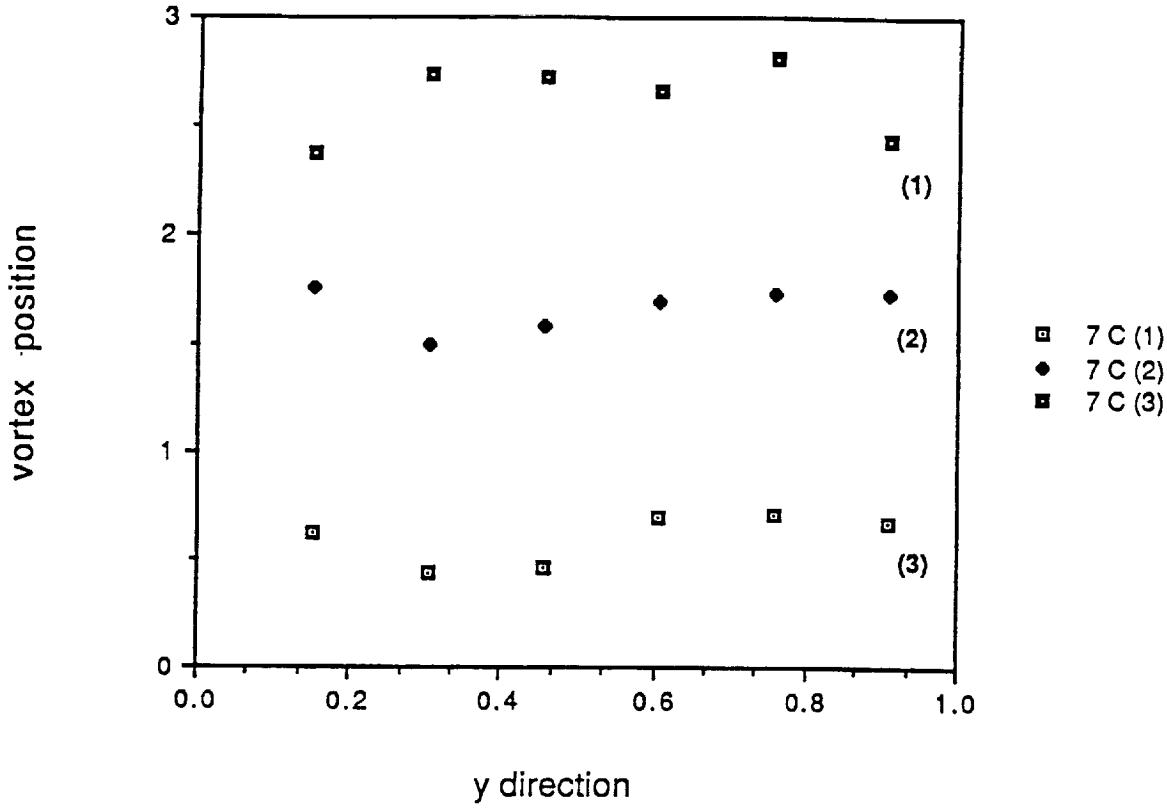

(Vertical axis shifted by one unit)